Carrier-Based Modulated Model Predictive Control for Vienna Rectifiers

Xu, Junzhong; Gao, Fei; Soeiro, Thiago Batista; Chen, Linglin; Tarisciotti, Luca ; Tang, Houjun ; Bauer, Pavol

Carrier-Based Modulated Model Predictive Control for Vienna Rectifiers

Junzhong Xu[1,2], Fei Gao[1,2], Thiago Batista Soeiro[3], Linglin Chen[4]
Luca Tarisciotti[5], Houjun Tang[1,2], Pavol Bauer[3]
1: *Department of Electrical Engineering*, *Shanghai Jiao Tong University*, Shanghai, China
2: *Key Laboratory of Control of Power Transmission and conversion, Shanghai Jiao Tong University,*
Ministry of Education, China
3: *DCE&S group*, *Delft University of Technology*, Delft, The Netherlands
4: *Huawei Technologies Co., Ltd*, Shenzhen, China
5: *Department of Engineering*, *Universidad Andres Bello*, Santiago, Chile
Junzhongxu@sjtu.edu.cn, fei.gao@sjtu.edu.cn, T.BatistaSoeiro@tudelft.nl
Timzjuuon@gmail.com, Luca.Tarisciotti@unab.cl, Hjtang@sjtu.edu.cn, P.Bauer@tudelft.nl
(*Corresponding author: Fei Gao*)

Keywords

≪MPC (Model-based Predictive Control)≫, ≪Modulation strategy≫, ≪Pulse Width Modulation (PWM)≫, ≪Voltage Source Converter (VSC)≫.

Abstract

The implementation of traditional finite-control-set model predictive control (FCS-MPC) with variable switching frequency in voltage source rectifiers (VSRs) can make the system suffer from poor current harmonics performance. In fact, the resulting wide-spread voltage harmonic generated at the AC terminals makes the design of the typical multi-order AC filtering bulky and prone to control instabilities. This paper proposed a fixed frequency carrier-based modulated model predictive control (CB-MMPC) which is able to overcome these issues. This control strategy aims to improve the total harmonic distortion (THD) of the AC current waveform without introducing any additional weight factor in the cost function of the optimization routine, while maintaining the typical performance of fast current dynamic response of the FCS-MPC. Herein, the detailed implementation of the proposed CB-MMPC is given, while considering its application to the current feedback control loop of a three-phase three-level Vienna rectifier. Finally, PLECS based simulation results are used to verify the feasibility and the effectiveness of the proposed control strategy and to benchmark its performance to the classical FCS-MPC strategy and the conventional application of a current closed loop implementing a proportional-integral(PI)-controller.

Introduction

The multiple versions of the three-phase three-level Vienna rectifiers are widely used in industry applications, such as telecommunication and data center power supplies [1], low power wind generation systems [2], electric vehicle battery chargers, and motor drives [3]. This unidirectional rectifier technology has many advantages over the conventional two-level rectifiers, i.e. it can achieve higher power density and lower cost due to the higher efficiency and simplified thermal management, and smaller AC filtering requirement because of the lower total harmonic distortion (THD) of the input currents [4, 5]. With the increasing utilization of Vienna rectifiers, the interest to the control scheme of this power electronic circuit has gained many momenta in both industry and academia [6, 7, 8]. A carrier-based space vector modulator for Vienna rectifiers is studied in [6], which is built based on the equivalence between the two- and three-level converters, which advantageously simplify its implementation in practice. Based on the existing knowledge on discontinuous pulse width modulation (PWM) methods for three-wire voltage source converters, many carrier-based implementations of discontinuous PWM (DPWM) methods suitable for a Vienna rectifier are proposed in [7, 8].

Among the aforementioned schemes, classic current feedback error compensator for Vienna rectifiers are mainly based on hysteresis, or the proportional-integral (PI), and the proportional-resonant (PR) controllers. Recently, with the advancement in digital signal processing technology [9], various model predictive control (MPC) methods have been proposed as replacement to the traditional current controllers with the aim to improve this variable dynamic response. A hybrid control scheme is proposed for the three-phase Vienna rectifier which combines the PI controller to obtain the desired output DC-link voltage and the finite-control-set MPC (FCS-MPC) to realize the AC current regulation and the necessary neutral point voltage balance [10]. In [11] for the application of a Vienna rectifier on a permanent magnet synchronous generator, the feasible eight vectors on each one of the six voltage sectors are used in a FCS-MPC concept. The FCS-MPC with discrete space-vector modulation (DSVM) has been proposed in [12], which selects the candidate vectors for the cost function depending on the magnitude of the reference voltage and achieves the high performance of both the low current ripple and fast dynamic response. Based on the DSVM in [12], an optimal DSVM-MPC method is proposed in [13] to improve the input current performance with lower computational calculation burden. However, since FCS-MPC utilizes only one switching state for the whole sampling interval, the controller will generate the output waveform with a variable switching frequency, making the design of harmonic and EMC filters which can satisfy stringent grid compliance standards more challenging.

To address this significant drawback, prior efforts have been made in multiple literatures, where the modulation technique is applied into MPC at a constant switching frequency [14, 15, 16, 17]. Adopting the space-vector modulation, modulated MPC (MMPC) is presented for three-phase two-level active rectifier in [14], which can remarkably reduce the AC current harmonic content. In [15], the error between the measured currents and the current references is used to calculate the times of the three vectors, i.e. two active vectors and a zero vector, resulting in a zero tracking error. A finite-set MPC strategy with fixed switching frequency is also developed in the grid-tied three-level neutral point-clamped converter [16] while the balance of the partial DC capacitor voltages was realized by utilizing the available redundant voltage vectors. According to the arm-voltage-regulating algorithm, a novel MMPC strategy especially suited for modular multilevel converters (MMC) is proposed with the aim to enhance the steady-state performance of the system under unbalanced grid conditions [17]. It is noted that so far very limited publications exist using the MMPC strategy in a Vienna rectifier, where the requirement of current distortion and dynamic response for its applications are strict [4, 5]. Therefore, a flexible MMPC method with the advantage of lower current distortion without sacrificing the performance of fast current dynamic response in MPC is worth of promotion in Vienna rectifiers.

In this paper a new carrier-based MMPC (CB-MMPC) strategy for Vienna rectifiers is proposed which do not compromises the typical performance of fast current dynamic response achieved in traditional MPC methods. Different from the traditional MMPC proposed in [14] and for the one used in the three-level neutral point-clamped converter in [16], the switching vectors which depend on the phase current directions is not always the same. Besides, it differs from the presented methods in [6, 7, 8] where the carrier-based PWM strategy is used, i.e. a modulation wave is compared with a triangular carrier wave and the intersections define the switching instants. From the implementation perspective the proposed MPC strategy is much simpler than the space-vector modulation approach as the involved computation burden is generally reduced [18]. This paper is structured as follows. First, the analytical model of the Vienna rectifiers is derived. Thereafter, the working principle of the proposed CB-MMPC strategy is illustrated. Finally a PLECS based simulation of a Vienna rectifier running the CB-MMPC is used to verify the effectiveness of the proposed method.

II. Modeling of a Three-phase Three-level Vienna Rectifier

A Vienna rectifier circuit is shown in Fig. 1. The basic converter is composed of a three-phase diode bridge, three four-quadrant switches (S_a, S_b, and S_c) connecting the input phases to the neutral point of the DC-bus M, two series-connected DC capacitors C_p and C_n, and boost inductors L at the grid side. Note that in Fig. 1, i_a, i_b and i_c represent the input currents of the Vienna rectifier, while u_{pn} is the output DC-link voltage. Assuming that each capacitor voltage is equal to half blueu_{pn}, then the
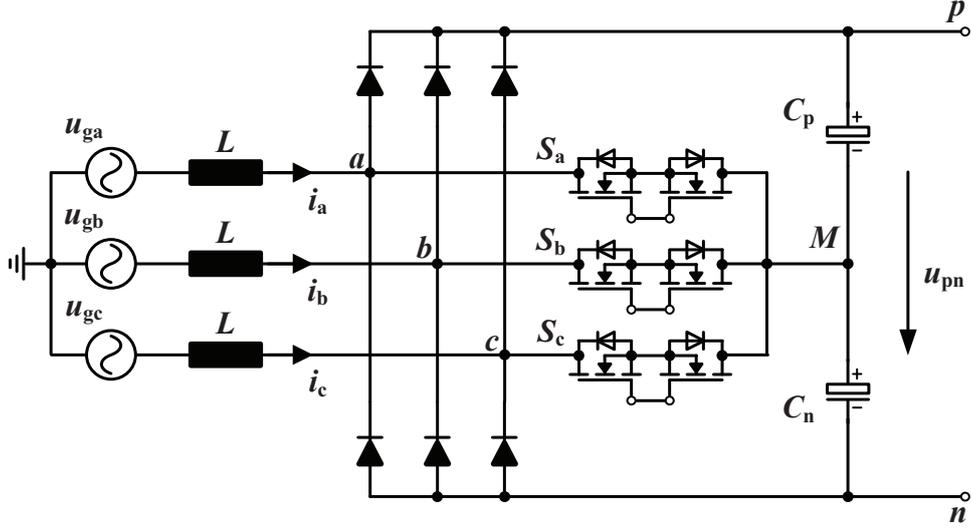
Fig. 1: Circuit schematic of a Vienna rectifier topology.

switching states of S_x ($x = a, b, c$) generate an AC voltage of $u_{xm} \in \{-u_{pn}/2, 0, u_{pn}/2\}$, i.e. the voltage of terminal $x = a, b, c$ with respect to the neutral point M as shown in Fig. 1. The switching states and the corresponding converter terminal voltages u_{xm} are summarized in Table I.

Table I: Switching States ($x = a, b, c$)

Phase current	S_x	u_{xm}	Voltage State
$i_x > 0$	0	$u_{pn}/2$	1
	1	0	0
$i_x > 0$	1	0	0
	0	$-u_{pn}/2$	-1

According to the impressed AC current flowing directions in Fig. 1, the input current (i_α and i_β) dynamics in α-β coordinate with the generated AC converter voltages ($u_{c\alpha}$ and $u_{c\beta}$) and grid voltages ($u_{g\alpha}$ and $u_{g\beta}$) are expressed as:

$$\begin{cases} L\frac{di_\alpha}{dt} = u_{g\alpha} - u_{c\alpha} \\ L\frac{di_\beta}{dt} = u_{g\beta} - u_{c\beta} \end{cases} \tag{1}$$

The currents through the DC-link capacitor can be expressed as:

$$\begin{cases} C_p \frac{du_{cp}}{dt} = i_{cp} \\ C_n \frac{du_{cn}}{dt} = i_{cn} \end{cases} \tag{2}$$

The derivative of the AC currents and the capacitor voltages in the continuous-time model can be approximated based on the forward Euler approximation with sampling period T_s as:

$$\frac{di_{\alpha\beta}}{dt} \approx \frac{i_{\alpha\beta}(k+1) - i_{\alpha\beta}(k)}{T_s} \tag{3}$$

$$\frac{du_c}{dt} \approx \frac{u_c(k+1) - u_c(k)}{T_s} \tag{4}$$

Fig. 2: Block diagram of the proposed CB-MMPC control scheme.

Thereafter, (1) and (2) can be re-written in the discrete form as:

$$\begin{cases} i_\alpha(k+1) = i_\alpha(k) + \frac{T_s}{L}[u_{g\alpha}(k) - u_{c\alpha}(k)] \\ i_\beta(k+1) = i_\beta(k) + \frac{T_s}{L}[u_{g\beta}(k) - u_{c\beta}(k)] \end{cases} \tag{5}$$

$$\begin{cases} u_{cp}(k+1) = u_{cp}(k) + \frac{T_s}{C_1}i_{cp}(k+1) \\ u_{cn}(k+1) = u_{cn}(k) + \frac{T_s}{C_2}i_{cn}(k+1) \end{cases} \tag{6}$$

III. Working Principle of The Proposed CB-MMPC

The proposed CB-MMPC includes a suitable modulation scheme in the cost function minimization. Fig. 2 shows the control block diagram of the CB-MMPC. Similar to the FCS-MPC strategy for the three-level neutral-point-clamped inverter in [16], it uses the prediction of the AC line currents and capacitor voltages based on (5) and (6), respectively. At every sampling time and depending on which one of the six current sectors the system operates, the CB-MMPC evaluates the parametric predictions of the two active and two redundant small vectors, and finally solves the cost function separately for each prediction to find the modulation waveform to compare with the carriers.

A. Vector Pre-selection

The converter voltage vectors are divided into six sectors according to the input three-phase current polarity as shown in Fig. 3(a), and the candidate voltage states to be applied in each sector are shown in Fig. 3(b). In fact, for a certain input current vector, there are only eight controllable voltage vectors.

Based on the conventional space-vector modulation, if the target vector is located in one triangle, then its vertice vectors are used to realize the target vector. One of the nearest vectors forming the triangle in question is always the redundant vector pointing to the center of the active hexagon. To reduce the number of the processed switching vectors, the candidate switching states (S_a, S_b, S_c) for six active vectors and two redundant vectors in each sector can be obtained by:

$$S_i^s = S_i^0 + 0.5[\text{sign}(i_x) - 1], \quad x \in \{a, b, c\}, \quad s \in \{1, 2 \ldots, 6\} \tag{7}$$

Fig. 3: Sector allocation and candidate voltage vectors for the three-level voltage source converter, (a) sector allocation, (b) candidate voltage vectors.

Table II: Feasible Switching Vectors in Sector I

Vector	(S_a^0, S_b^0, S_c^0)	(S_a^1, S_b^1, S_c^1)
$\mathbf{V}_0^1$	(0, 0, 0)	(0, -1, -1)
$\mathbf{V}_1^1$	(0, 0, 1)	(0, -1, 0)
$\mathbf{V}_2^1$	(0, 1, 0)	(0, 0, -1)
$\mathbf{V}_3^1$	(0, 1, 1)	(0, 0, 0)
$\mathbf{V}_4^1$	(1, 0, 0)	(1, -1, -1)
$\mathbf{V}_5^1$	(1, 0, 1)	(1, -1, 0)
$\mathbf{V}_6^1$	(1, 1, 0)	(1, 0, -1)
$\mathbf{V}_7^1$	(1, 1, 1)	(1, 0, 0)

where (S_a^0, S_b^0, S_c^0) is the basic switching state from (0, 0, 0) to (1, 1, 1). $\text{sign}(i_x) = 1$ when $i_x \geq 0$, otherwise $\text{sign}(i_x) = -1$. Taking sector I as an example ($i_a > 0$, $i_b < 0$, and $i_c < 0$), the only eight candidate switching states are summarized in Table II. The candidate switching sates in another sector can be pre-selected by (7) in the same way.
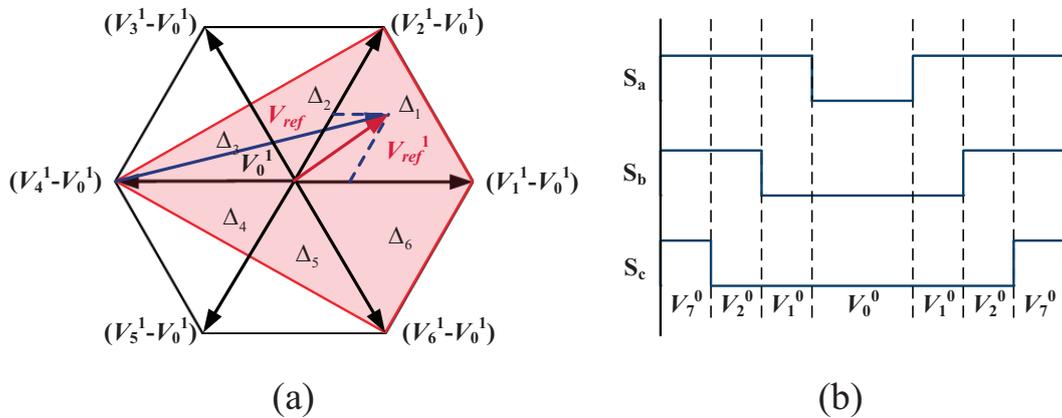
Fig. 4: Implementation of the CB-MMPC in sector I (a) equivalent reference voltage vector in two-level space vector diagram (b) switching pattern.

Once the sector is determined, the origin of a reference voltage vector can be changed to the center voltage vector of the selected hexagon $\mathbf{V}_0^s$. This is done by subtracting the center vector of the selected

hexagon from the original reference vector $\mathbf{V}_0^s$, as shown in Fig. 4(a). The space vector diagram of each sector shown in Fig. 4(a) is divided into 6 triangles (denoted as Δ_n with $n \in \{1,...,6\}$), where each triangle Δ_n is composed of two equivalent active vectors $\mathbf{V}_i^0$ and $\mathbf{V}_j^0$ ($i, j \in \{1,2...6\}$ $\mathbf{V}_{i,j}^0 = \mathbf{V}_{i,j}^s - V_0^s$). For the implementation of the SVPWM, a symmetrical pulse pattern is adopted in this work, as shown in Fig. 4(b).

B. Converter Voltage Reference Calculations

Based on (5), the current predictions can be rewritten as:

$$
\begin{cases}
i_\alpha(k+1) = i_\alpha^0(k+1) - \frac{T_s}{L}[d_i(\mathbf{V}_{\alpha i}^s - \mathbf{V}_{\alpha 0}^s) + d_j(\mathbf{V}_{\alpha j}^s - \mathbf{V}_{\alpha 0}^s)] \\
i_\beta(k+1) = i_\beta^0(k+1) - \frac{T_s}{L}[d_i(\mathbf{V}_{\beta i}^s - \mathbf{V}_{\beta 0}^s) + d_j(\mathbf{V}_{\beta j}^s - \mathbf{V}_{\beta 0}^s)]
\end{cases}
\tag{8}
$$

$$
\Rightarrow
\begin{cases}
i_\alpha(k+1) = i_\alpha^0(k+1) - \frac{T_s}{L}(d_i \mathbf{V}_{\alpha i}^0 + d_j \mathbf{V}_{\alpha j}^0) \\
i_\beta(k+1) = i_\beta^0(k+1) - \frac{T_s}{L}(d_i \mathbf{V}_{\beta i}^0 + d_j \mathbf{V}_{\beta j}^0)
\end{cases}
\tag{9}
$$

where (i_α^0, i_β^0) represents the evolution of the system, when the redundant vector $\mathbf{V}_0^s$ is applied, and d_i and d_j are duty cycles of the selected active vector $\mathbf{V}_i^s$ and $\mathbf{V}_j^s$. Assuming that the predicted currents match the current references, the voltage references $(\mathbf{V}_\alpha^*, \mathbf{V}_\beta^*)$ can be defined as:

$$
\begin{cases}
\mathbf{V}_\alpha^*(k+1) = \frac{L}{T_s}[i_\alpha^0(k+1) - i_\alpha^*(k+1)] \\
\mathbf{V}_\beta^*(k+1) = \frac{L}{T_s}[i_\beta^0(k+1) - i_\beta^*(k+1)].
\end{cases}
\tag{10}
$$

C. Current prediction and duty cycle calculation

According to Table II, the current predictions are calculated for each one of the candidate adjacent vectors $(\mathbf{V}_i^0, \mathbf{V}_j^0)$ considering both vectors applied in one sampling interval:

$$
\begin{cases}
i_\alpha^i(k+1) = i_\alpha^0(k+1) - \frac{T_s}{L} d_i \mathbf{V}_{\alpha i}^0 \\
i_\beta^i(k+1) = i_\beta^0(k+1) - \frac{T_s}{L} d_i \mathbf{V}_{\beta i}^0
\end{cases}
\tag{11}
$$

$$
\begin{cases}
i_\alpha^j(k+1) = i_\alpha^0(k+1) - \frac{T_s}{L} d_j \mathbf{V}_{\alpha j}^0 \\
i_\beta^j(k+1) = i_\beta^0(k+1) - \frac{T_s}{L} d_j \mathbf{V}_{\beta i}^0
\end{cases}
\tag{12}
$$

The duty cycles are calculated based on the voltage reference derived from (10) for each one of the two active vectors:

$$
\begin{cases}
\mathbf{V}_\alpha^* = d_i \mathbf{V}_{\alpha i}^0 + d_j \mathbf{V}_{\alpha j}^0 + \mathbf{V}_{\alpha 0}^s \\
\mathbf{V}_\beta^* = d_i \mathbf{V}_{\beta i}^0 + d_j \mathbf{V}_{\beta j}^0 + \mathbf{V}_{\beta 0}^s
\end{cases}
\tag{13}
$$

Solving the above equation, the duty cycles for each pair of vectors can be defined by:

$$
\begin{cases}
d_i = \frac{(\mathbf{V}_\beta^* - \mathbf{V}_{\beta 0}^s)\mathbf{V}_{\alpha j}^0 - (\mathbf{V}_\alpha^* - \mathbf{V}_{\alpha 0}^s)\mathbf{V}_{\beta j}^0}{\mathbf{V}_{\alpha j}^0 \mathbf{V}_{\beta j}^0 - \mathbf{V}_{\alpha i}^0 \mathbf{V}_{\beta j}^0} \\
d_j = \frac{(\mathbf{V}_\beta^* - \mathbf{V}_{\beta 0}^s)\mathbf{V}_{\alpha i}^0 - (\mathbf{V}_\alpha^* - \mathbf{V}_{\alpha 0}^s)\mathbf{V}_{\beta i}^0}{\mathbf{V}_{\alpha i}^0 \mathbf{V}_{\beta j}^0 - \mathbf{V}_{\alpha j}^0 \mathbf{V}_{\beta i}^0}
\end{cases}
\tag{14}
$$

Thereafter, the duty cycle of the selected center voltage vector d_0 can be calculated by:

$$
d_0 = 1 - d_i - d_j.
\tag{15}
$$

D. Cost Function Minimization and Capacitor Voltage Balancing

A single-objective predictive controller regulates the grid currents using the following cost function:

$$G = G_i + G_j$$
$$G_i = d_i\sqrt{(i_\alpha^i - i_\alpha^*)^2 + (i_\beta^i - i_\beta^*)^2}$$
$$G_j = d_j\sqrt{(i_\alpha^j - i_\alpha^*)^2 + (i_\beta^j - i_\beta^*)^2}$$

(16)

The pair of vectors with the minimum value of G is selected to be applied for the associated duty cycles d_i and d_j.

Negative and positive small vectors $\mathbf{V}_0^0$ and $\mathbf{V}_7^0$ have an opposite effect in the current injected at the neutral-point terminal M. The ratio between the negative and positive duty cycles are redistributed as a function of the following imbalance index:

$$\Delta u_b = \frac{u_{cp} - u_{cn}}{u_{cp} + u_{cn}}$$

(17)

which is bounded between (-1, 1). Thus, duty cycles of $\mathbf{V}_0^0$ and $\mathbf{V}_7^0$ are calculated as follows:

$$d_0^- = \frac{1 - \Delta u_b}{2} d_0$$

(18)

$$d_0^+ = \frac{1 + \Delta u_b}{2} d_0$$

(19)

E. Modulation Waveforms Generation

The optimal pair of vectors $\mathbf{V}_i^0$ and $\mathbf{V}_j^0$ with the minimum value of G obtained from (16), whose equivalent switching state $(S_{ai}^0, S_{bi}^0, S_{ci}^0)$ and $(S_{aj}^0, S_{bj}^0, S_{cj}^0)$ is selected to be applied to the associated duty cycles d_a, d_b, and d_c.

$$\begin{cases} d_a = d_i S_{ai}^0 + d_j S_{aj}^0 + d_0^+ \\ d_b = d_i S_{bi}^0 + d_j S_{bj}^0 + d_0^+ \\ d_c = d_i S_{ci}^0 + d_j S_{cj}^0 + d_0^+ \end{cases}$$

(20)

Finally, the modulation waveforms u_a^*, u_b^*, and u_c^* that are set to be compared to the triangular carriers are obtained as:

$$\begin{cases} u_a^* = 2d_a - 1 \\ u_b^* = 2d_b - 1 \\ u_c^* = 2d_c - 1 \end{cases}$$

(21)

IV. Simulation Results

To validate the effectiveness of the proposal CB-MMPC in a Vienna rectifier, PLECS based simulation results are presented during both steady-state and dynamic test conditions. These results are compared with the ones obtained with the same converter employing the classical FCS-MPC strategy or the traditional PI-controller. The grid voltage is set as $220V_{rms}$; the value of inductance is $360\,\mu H$; the switching and sampling frequency are 20 kHz.

The steady-state waveforms for the three-phase grid currents, the converter generated terminal voltage u_{am}, and the current harmonic spectrum obtained with the proposed MMPC, the conventional FCS-MPC, and the PI-controller are shown in Fig. 5, where the output voltage is 800 V, and resistive load is 50 Ω. From the current spectrum analysis, one can observe that the proposed CB-MMPC produces a current

with a constant switching frequency of 20 kHz as the one with PI controller, while the FCS-MPC control has a variable switching frequency, which is mostly lower than 20 kHz.
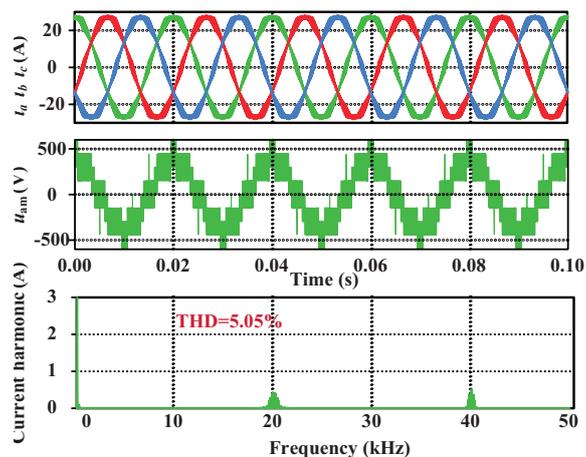
(a)
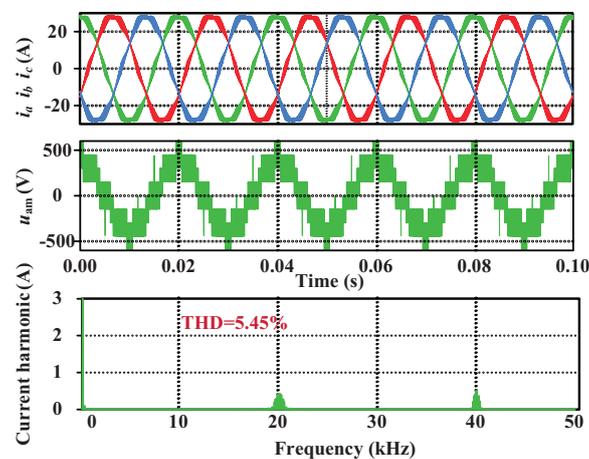
(b)
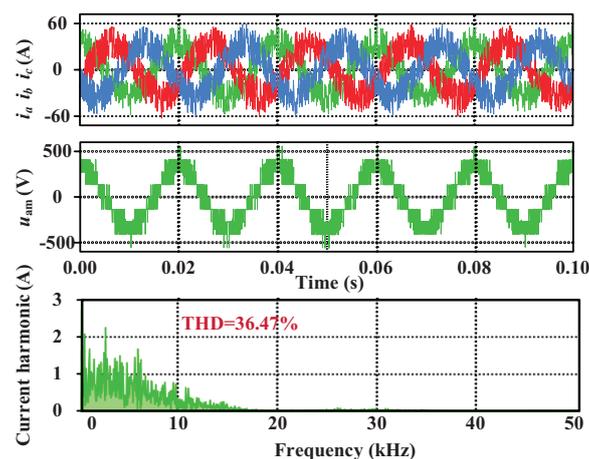
(c)

Fig. 5: Steady-state simulation waveforms of the grid currents, the terminal voltage u_{am}, and phase current harmonics for implementation of (a) the proposed MMPC, (b) the PI-controller, (c) the conventional FCS-MPC.

Fig. 6 shows the dynamic behavior of the three studied methods when the DC-link voltage reference is 800V and the load changes from 100 Ω to 50 Ω at t = 0.1s. The parameters in the voltage-PI-controller

for the three methods are exactly the same. It can be seen that u_{pm} drops more for PI-controller than the other two predictive-based controllers in the presence of the load disturbance. Both predictive control methods have a faster dynamics response than the PI-controller.
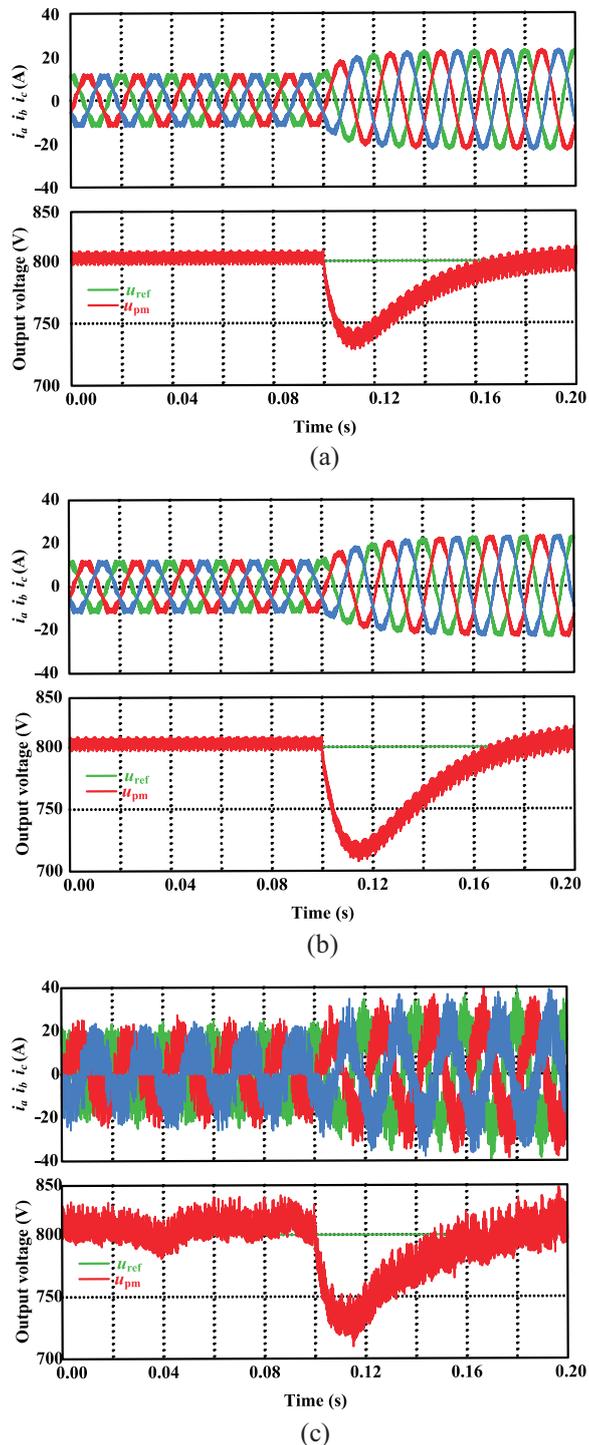
Fig. 6: Dynamic simulation waveform of grid currents, output voltage u_{pm} and its reference u_{ref} (a) the proposed MMPC, (b) the PI-controller, (c) the conventional FCS-MPC.

Conclusion

This paper has proposed a carrier-based modulated model predictive control (CB-MMPC) with fixed switching frequency for a three-phase Vienna rectifier. This control method implements a CB-MMPC

with sector pre-selection, where the number of finite switching states of the rectifier under different current conditions are determined. Compared with the classic FCS-MPC, it solves the problem of the converter generation of a wide spectrum of voltage/current harmonic content without affecting the control performance in terms of fast dynamic response. PLECS based simulations have verified the effectiveness and superiority of the proposed CB-MMPC method.

References

[1] J. W. Kolar and F. C. Zach: A novel three-phase utility interface minimizing line current harmonics of high-power telecommunications rectifier modules, IEEE Transactions on Industrial Electronics,Vol. 44, no. 4, pp. 456-467

[2] A. Rajaei, M. Mohamadian and A. Yazdian Varjani: Vienna-Rectifier-Based Direct Torque Control of PMSG for Wind Energy Application, IEEE Transactions on Industrial Electronics, vol. 60, no. 7, pp. 2919-2929

[3] R. Lai et al.: A Systematic Topology Evaluation Methodology for High-Density Three-Phase PWM AC-AC Converters, IEEE Transactions on Power Electronics, vol. 23, no. 6, pp. 2665-2680

[4] J. W. Kolar and T. Friedli: The Essence of Three-Phase PFC Rectifier SystemsPart I, IEEE Transactions on Power Electronics, vol. 28, no. 1, pp. 176-198,

[5] T. Friedli, M. Hartmann and J. W. Kolar: The Essence of Three-Phase PFC Rectifier SystemsPart II, IEEE Transactions on Power Electronics, vol. 29, no. 2, pp. 543-560

[6] R. Burgos, R. Lai, Y. Pei, F. Wang, D. Boroyevich and J. Pou: Space Vector Modulator for Vienna-Type RectifiersBased on the Equivalence BetweenTwo- and Three-Level Converters:A Carrier-Based Implementation, IEEE Transactions on Power Electronics, vol. 23, no. 4, pp. 1888-1898

[7] J. Lee and K. Lee: Carrier-Based Discontinuous PWM Method for Vienna Rectifiers, IEEE Transactions on Power Electronics, vol. 30, no. 6, pp. 2896-2900

[8] J. Lee and K. Lee: Performance Analysis of Carrier-Based Discontinuous PWM Method for Vienna Rectifiers With Neutral-Point Voltage Balance, IEEE Transactions on Power Electronics, vol. 31, no. 6, pp. 4075-4084

[9] S. Kouro, P. Cortes, R. Vargas, U. Ammann and J. Rodriguez: Model Predictive ControlA Simple and Powerful Method to Control Power Converters, IEEE Transactions on Industrial Electronics, vol. 56, no. 6, pp. 1826-1838

[10] X. Li, Y. Sun, H. Wang, M. Su and S. Huang: A Hybrid Control Scheme for Three-Phase Vienna Rectifiers, IEEE Transactions on Power Electronics, vol. 33, no. 1, pp. 629-640

[11] J. Lee and K. Lee: Predictive Control of Vienna Rectifiers for PMSG Systems, IEEE Transactions on Industrial Electronics, vol. 64, no. 4, pp. 2580-2591

[12] J. Lee, K. Lee and F. Blaabjerg: Predictive Control With Discrete Space-Vector Modulation of Vienna Rectifier for Driving PMSG of Wind Turbine Systems, IEEE Transactions on Power Electronics, vol. 34, no. 12, pp. 12368-12383

[13] W. Zhu, C. Chen and S. Duan: Model predictive control with improved discrete space vector modulation for three-level Vienna rectifier, IET Power Electronics, vol. 12, no. 8, pp. 1998-2004

[14] L. Tarisciotti, P. Zanchetta, A. Watson, J. C. Clare, M. Degano and S. Bifaretti: Modulated Model Predictive Control for a Three-Phase Active Rectifier, IEEE Transactions on Industry Applications, vol. 51, no. 2, pp. 1610-1620

[15] E. Fuentes, C. A. Silva and R. M. Kennel: MPC Implementation of a Quasi-Time-Optimal Speed Control for a PMSM Drive, With Inner Modulated-FS-MPC Torque Control, IEEE Transactions on Industrial Electronics, vol. 63, no. 6, pp. 3897-3905

[16] F. Donoso, A. Mora, R. Crdenas, A. Angulo, D. Sez and M. Rivera: Finite-Set Model-Predictive Control Strategies for a 3L-NPC Inverter Operating With Fixed Switching Frequency, IEEE Transactions on Industrial Electronics, vol. 65, no. 5, pp. 3954-3965

[17] Z. Gong, X. Wu, P. Dai and R. Zhu: Modulated Model Predictive Control for MMC-Based Active Front-End Rectifiers Under Unbalanced Grid Conditions, IEEE Transactions on Industrial Electronics, vol. 66, no. 3, pp. 2398-2409

[18] A. Cataliotti, F. Genduso, A. Raciti and G. R. Galluzzo: Generalized PWMVSI Control Algorithm Based on a Universal Duty-Cycle Expression: Theoretical Analysis, Simulation Results, and Experimental Validations, IEEE Transactions on Industrial Electronics, vol. 54, no. 3, pp. 1569-1580